

# Active Brazing of C/C Composite to Copper by AgCuTi Filler Metal



KEXIANG ZHANG, LIHONG XIA, FUQIN ZHANG, and LIANLONG HE

Brazing between the carbon–fiber–reinforced carbon composite (C/C composite) and copper has gained increasing interest because of its important application in thermal management systems in nuclear fusion reactors and in the aerospace industry. In order to examine the “interfacial shape effect” on the mechanical properties of the joint, straight and conical interfacial configurations were designed and machined on the surface of C/C composites before joining to copper using an Ag-68.8Cu-4.5Ti (wt pct) alloy. The microstructure and interfacial microchemistry of C/C composite/AgCuTi/Cu brazed joints were comprehensively investigated by using high-resolution transmission electron microscopy. The results indicate that the joint region of both straight and conical joints can be described as a bilayer. Reaction products of  $\text{Cu}_3\text{Ti}_3\text{O}$  and  $\gamma\text{-TiO}$  were formed near the copper side in a conical interface joint, while no reaction products were found in the straight case. The effect of Ag on the interfacial reaction was discussed, and the formation mechanism of the joints during brazing was proposed. On the basis of the detailed microstructure presented, the mechanical performance of the brazed joints was discussed in terms of reaction and morphology across the joint.

DOI: 10.1007/s11661-016-3340-y

© The Minerals, Metals & Materials Society and ASM International 2016

## I. INTRODUCTION

CARBON-FIBER-REINFORCED carbon composites (C/C composites) have been widely used in many areas due to their superior thermal and mechanical properties at high temperatures.<sup>[1,2]</sup> However, some applications in the aerospace and nuclear industries will require joining such C/C composites to metals or alloys. For example, diverters used in the International Thermonuclear Experimental Reactor need C/C composites to be joined to the copper alloy as part of the lower vertical target.<sup>[3]</sup> There are several ways to join C/C composites to metals, including direct casting after surface modification of C/C composites and active brazing.<sup>[4,5]</sup> Brazing is one of the most popular methods for joining C/C composites to metals or other substrates, since it has many advantages such as low brazing temperature, low pressure, and low residual stress in the joints. Therefore, there has been considerable interest in brazing C/C composites to different metals or other substrates using different filler metals in recent years due

to their technological importance.<sup>[6]</sup> There are usually two problems that deteriorate the quality of brazing of C/C composites to metals or alloys. One is the wettability of the carbon surface by liquid metals or alloys. The wettability of carbon has been partly improved by adding the active element Ti to the braze alloy, which has a strong affinity to carbon. Modification of C/C composites is also feasible in order to obtain a carbide coating wettable by metal through the slurry technique.<sup>[7]</sup> The other one is the residual thermal stress in the joint, caused mainly by the mismatch of the coefficient of thermal expansion (CTE) between C/C composites and metal/alloy substrates. For example, the CTE for C/C composites is less than  $1.0 \times 10^{-6} \text{ K}^{-1}$  in the temperature range 293 K to 523 K (20 °C to 250 °C) and 2.0 to approximately  $4.0 \times 10^{-6} \text{ K}^{-1}$  in the range 293 K to 2773 K (20 °C to 2500 °C),<sup>[8]</sup> for pure copper, the CTE is 16 to approximately  $20 \times 10^{-6} \text{ K}^{-1}$ . The CTE discrepancy between them is rather large. Two methods have been used to release the residual thermal stress of the joints. One technique is inserting a soft metal foil between every two braze foils to transfer thermal stress,<sup>[9]</sup> the other process is geometry modification on the surface of C/C composite. Wang *et al.*<sup>[10]</sup> modified the joint surface of C/C composites by drilling holes on the surface. The results show that such surface puncturing can significantly improve the strength of the joint. Shen *et al.*<sup>[11]</sup> obtained the zigzag interfacial structure by means of micromachining the joint surface, which also enhanced the joint strength.

In recent years, various active filler materials, especially Ag- and Cu-based filler alloys, were developed, including commercial active metal braze, such as Cu-ABA (2.25 wt pct Ti), Cusil-ABA (1.75 wt pct Ti), Ticusil

KEXIANG ZHANG, Ph.D. Student, is with Shenyang National Laboratory for Materials Science, Institute of Metal Research, Chinese Academy of Sciences, Shenyang 110016, China, and also with the University of Chinese Academy of Sciences, Beijing 100049, China. LIHONG XIA, Ph.D. Student, and FUQIN ZHANG, Professor, are with the National Key Laboratory of Science and Technology on High-strength Lightweight Structural Materials, Central South University, Changsha 410083, China. LIANLONG HE, Professor, is with the Shenyang National Laboratory for Materials Science, Institute of Metal Research, Chinese Academy of Sciences. Contact e-mail: llhe@imr.ac.cn

Kexiang Zhang, and Lihong Xia have contributed equally to this work.

Manuscript submitted July 18, 2015.

Article published online March 1, 2016

(4.5 wt pct Ti), and Ticuni (70 wt pct Ti).<sup>[1,7,12,13]</sup> The Ag- and Cu-based filler alloys containing active element Ti are the most frequently used braze to join C/C composites to metals or other substrates, since these systems have better braze spreading, which leads to larger bonded areas.<sup>[1,3]</sup> In fact, the alloys of the Ag-Cu-Ti system have been extensively used in ceramic/metal joining applications in the temperature range 1073 K to 1173 K (800 °C to 900 °C).<sup>[14]</sup> It is believed that the role of the active Ti element is to change the chemistry of the carbon surface by *in situ* reaction with carbon and, thus, to increase wettability and adhesion. It was proven that even a small addition of titanium in copper or silver can decrease the contact angle on carbon intensely.<sup>[15]</sup>

Microstructures of the brazed joints formed using Cu- or Ag-based fillers containing titanium were widely investigated.<sup>[2,13,16]</sup> In that research, most of the microstructural characterizations of the brazed joints were investigated by scanning electron microscopy (SEM), and the redistribution of alloying elements and reaction products were examined by energy-dispersive X-ray spectrometry (EDS). Because of the limitation of SEM resolution and the thickness of the SEM sample, details can seldom be obtained on the nanometer scale. In the present study, the C/C composite/AgCuTi/Cu brazed joints were investigated on the nanometer scale by using high-resolution transmission electron microscopy (TEM) with EDS. Detailed microstructures of the joints were reported, with the purpose of examining the effect of microstructure and interface shape on the mechanical properties of the joints, which could be meaningful for the brazing process optimization.

## II. EXPERIMENT

### A. Brazing Process and Characterization of the Joints

This Quasi-3D C/C composite was offered by HUNAN BOYUN NEW MATERIALS CO., LTD. in Changsha, China. The needled felt preform was fabricated by needling the stack of alternating layers of unidirectional nonwoven carbon cloth and short-cut-fiber webs with a needle-punching technique in the Z direction using PAN T-300C fibers (Toray Industries Inc, Japan). The preform was first densified by the chemical vapor deposition (CVD) process followed by resin impregnation and carbonization. The density of the C/C composite was about 1.8 g/cm<sup>3</sup> after densification. The Cu substrate was cathode copper, and the purity was not less than 99.95 pct. The nominal chemical composition of the copper-based active brazing foils was Ag-68.8Cu-4.5Ti (wt pct). The thickness of the foils was about 150 μm. The C/C composite and the copper were cut into 16 mm × 16 mm × 20 mm rectangular solids, the braze foil was also cut into 16 mm × 16 mm pieces. The nonwoven cloth layers were perpendicular to the joining surface. The joining surfaces of both the C/C composite and copper were ground by 400-, 600-, 800-, and 1000-grit silicon carbide paper step-by-step, respectively. Then all of the materials were ultrasonically cleaned with acetone for 10 minutes and then with

ethanol for another 10 minutes prior to their use. The braze foil was sandwiched between them. Brazing was processed at 1183 K (910 °C) for 10 minutes under the vacuum of less than  $5 \times 10^{-3}$  Pa. The heating rate was 10 °C/minute. The cooling rate was set as 3 °C/minute from 1183 K to 773 K (910 °C to 500 °C), and the sample was held for 1 hour at 773 K (500 °C). Finally, it was furnace cooled to room temperature. For optical microscopy (OM) and SEM observation, the brazed joints were sectioned perpendicular to the bonded interface, followed by grinding with silicon carbide paper and polishing. The SEM examination was done on FEI Inspect<sup>TM</sup> F50. For TEM investigation, the thin films of the brazing zone were prepared cross sectionally by grinding the samples with a thickness of about 1.0 mm down to 20 to 30 μm; the ground samples were then dimpled for 20 minutes before ion milling. TEM observations were carried out with a JEM-2100 high-resolution TEM with point resolution of 0.25 nm and an FEI Tecnai<sup>TM</sup> G2 F30 high-spatial resolution TEM with point resolution of 0.2 nm.

### B. Mechanical Property Test

The brazed joints were cut 4 mm × 5 mm × 40 mm for four-point bending strength tests. The four-point bending strength tests of brazed joints were performed on an INSTRON-1342 Electro-hydraulic servo control material testing machine. The stress field in the sample strongly depends on the test configuration. The configuration for the bending strength test is schematically shown in Figure 1. The brazed joints were compressed with a constant loading rate of 0.5 mm/minute. The strength of the joint was given by  $\sigma = \frac{3P(L-I)}{2bd^2}$ , where  $\sigma$  is the four-point bending strength (MPa),  $P$  is the maximum load when joints fracture (N),  $L$  is the distance between the sample supports (mm),  $I$  is the distance between the pressure heads (mm),  $b$  is the width of the sample (mm), and  $d$  is the height of the sample (mm).

## III. RESULTS

### A. Interfacial Design and Interface Morphology

Two kinds of surfaces of C/C composite, straight and conical, were designed and machined, as shown in Figure 2, so that there were two kinds of interfaces

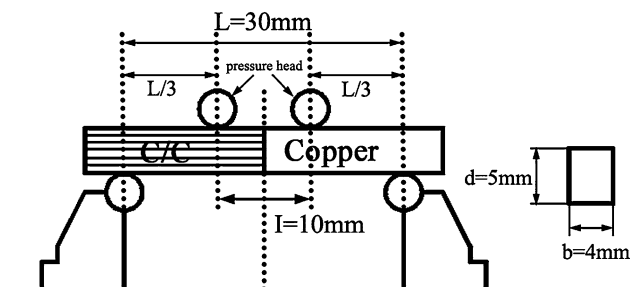


Fig. 1—Schematic configuration of four-point bending strength tests.

formed between C/C composites and copper: a straight interface (Figure 2(a)) and a conical interface (Figure 2(b)). For the conical one, cones were arranged as  $4 \times 4$  cones in a  $16 \text{ mm} \times 16 \text{ mm}$  square; every two adjacent cones were tangent at a basal circle (shown in Figure 2(c)). Figure 2(d) is the longitudinal-section view of the conical structure and indicates that the diameter and height of the cones are 3.2 and 2.0 mm, respectively.

The brazing conditions for these two designed interfaces were the same. Figure 3(a) shows the typical macroscopic appearance of the brazed joint. There is no apparent difference between the straight and conical interface brazed joints. Figures 3(b) and (c) show the typical metallographic section views of the straight and conical interface joints, respectively. The inserts show the characteristic of each joint. The straight interface between the C/C composite and copper can be seen in Figure 3(b). In Figure 3(c), it can be seen that the conical interface shows a zigzag structure (insert) as a result of the “stab cone structure” design.

Both of the joints brazed soundly well, although sometimes “welding lines” were seen in the brazing zone for the straight interface joint. It can be seen that the brazing alloy leads to good bonding between either the C/C composite and the brazing zone or the brazing zone and copper, without obvious defects such as voids and cracks. There is a wide interfacial diffusive-reactive region between copper and the C/C composite. The joint region in the conical interface is rather wider than in the straight interface case due to the infiltration of the conical area.

## B. Microstructure of the Joints

The SEM micrograph of the joints in Figure 4 shows that the two joints have the same microstructure characteristic. The brazing zone typically consists of two layers: layer I bordering the C/C composite has a large area; and layer II, which is a layer hundreds of micrometers thick, forms in contact with copper. The thickness of layer I in the conical interface is obviously larger than the straight interface due to the conical interface design. In the case of the straight interface, the thickness of layer II is about  $500 \mu\text{m}$ , while in the conical case, the thickness of layer II is about  $400 \mu\text{m}$ . The details of the extensive microstructural characterization of these two layers and the interface microstructure between the C/C composite and brazing zone are given in Sections I and II.

### 1. Microstructure of layer I

Extensive observation revealed that layer I in both the straight and conical interface joints had similar microstructure. Therefore, only the microstructures of layer I for the conical interface were presented in detail. Figure 5(a) shows the overview morphology of layer I. It can be seen that this layer is composed of gray and white zones. A magnified micrograph in Figure 5(b) shows that, in addition to the obvious gray (marked A) and white zones (marked B), there are also numerous small irregular gray blocks (marked C) dispersed in white zones. The EDS analyses results (here the content of element C is neglected) shown in Table I indicate that

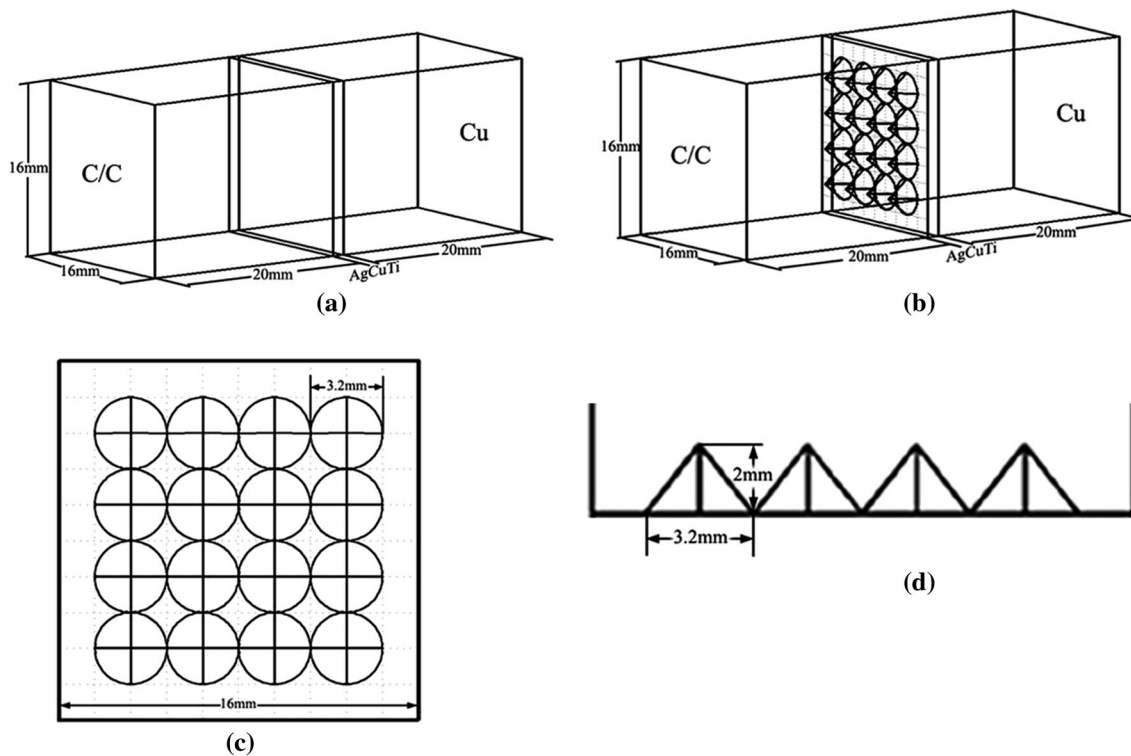


Fig. 2—Schematic diagrams of the brazing assembly of C/C composite/AgCuTi/Cu joint. (a) Surface of C/C composite at the interface is flat; (b) surface of C/C composite at the interface was machined into conical structure, showing the stab cone structure; (c) arranged configuration of the cones; and (d) longitudinal-section view of the conical structure. The basal diameter and height of the cones are 3.2 and 2 mm, respectively.



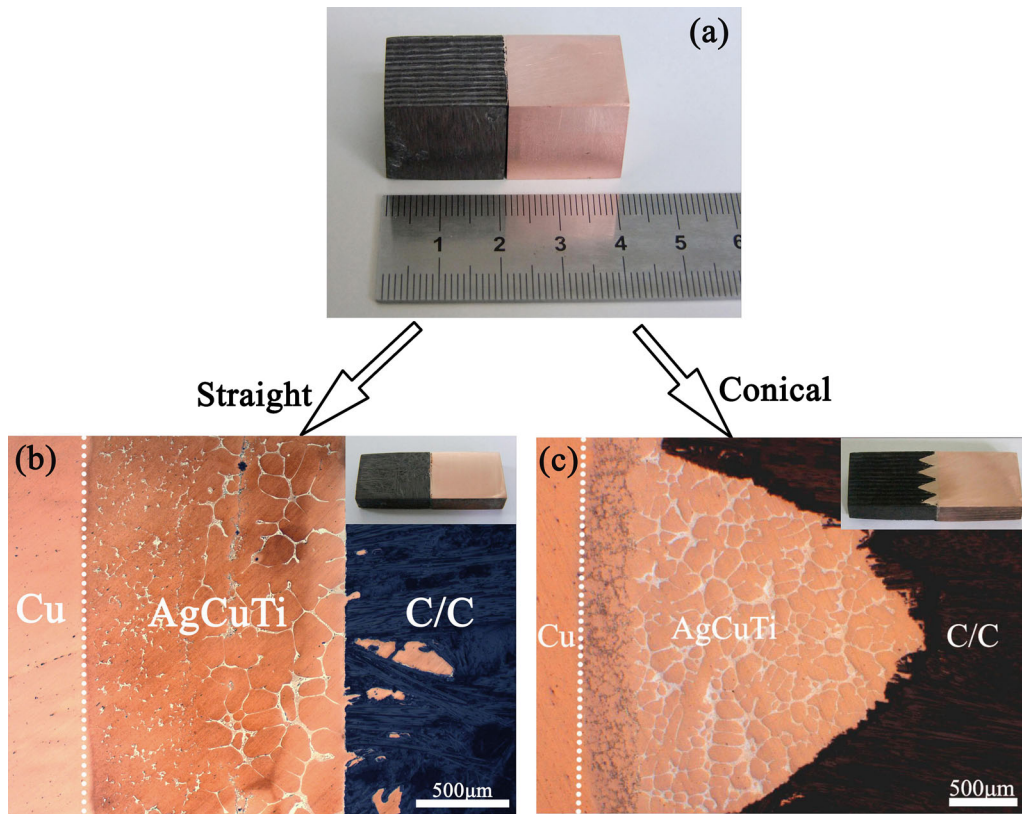


Fig. 3—(a) Macroscopic appearance of the brazed C/C composite/AgCuTi/Cu joints. There is no difference from the outside surface between straight and conical interface brazed joints. (b) and (c) OM views of straight and conical interface joints, respectively. Insets show that the interface for the straight interface joint is flat, while the conical interface shows a zigzag structure due to the conical design.

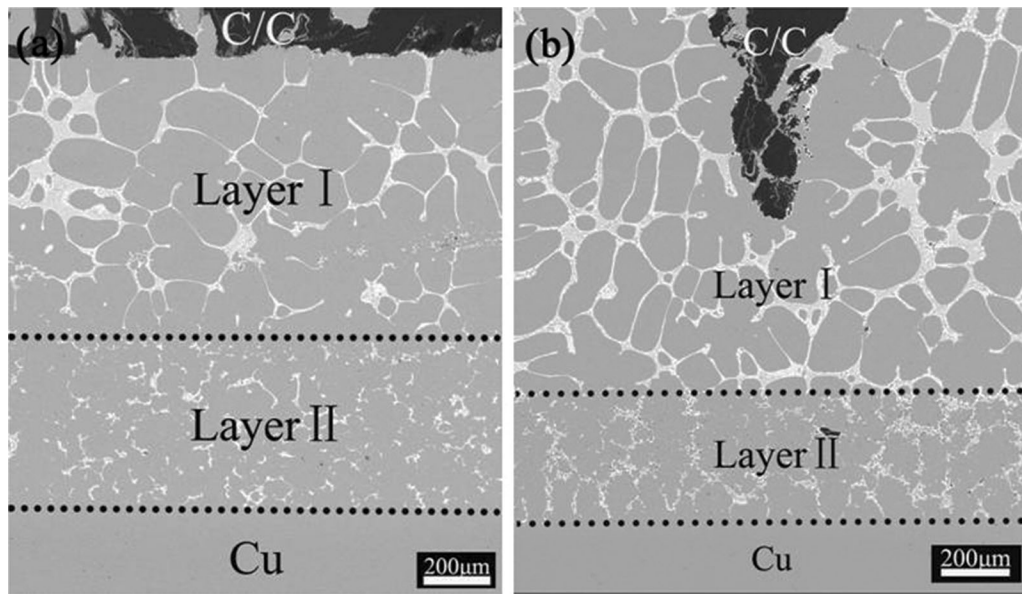


Fig. 4—(a) and (b) Typical SEM micrographs of the straight and conical interface joints, respectively; the brazing zone of both joints typically consists of two layers from the morphology characteristic.

zones A and B are rich in elements Cu and Ag, respectively, while zone C is also Cu rich. According to Ag-Cu, Cu-Ti, and Ag-Ti phase diagrams, zones A and C are probably Cu-based solid solution and zone B

is probably Ag-based solid solution. In this region, the Ti concentration is rather low (only a small quantity of Ti dissolved in Cu solid solution) and the solidification process is similar to the Ag-Cu alloy with hypereutectic

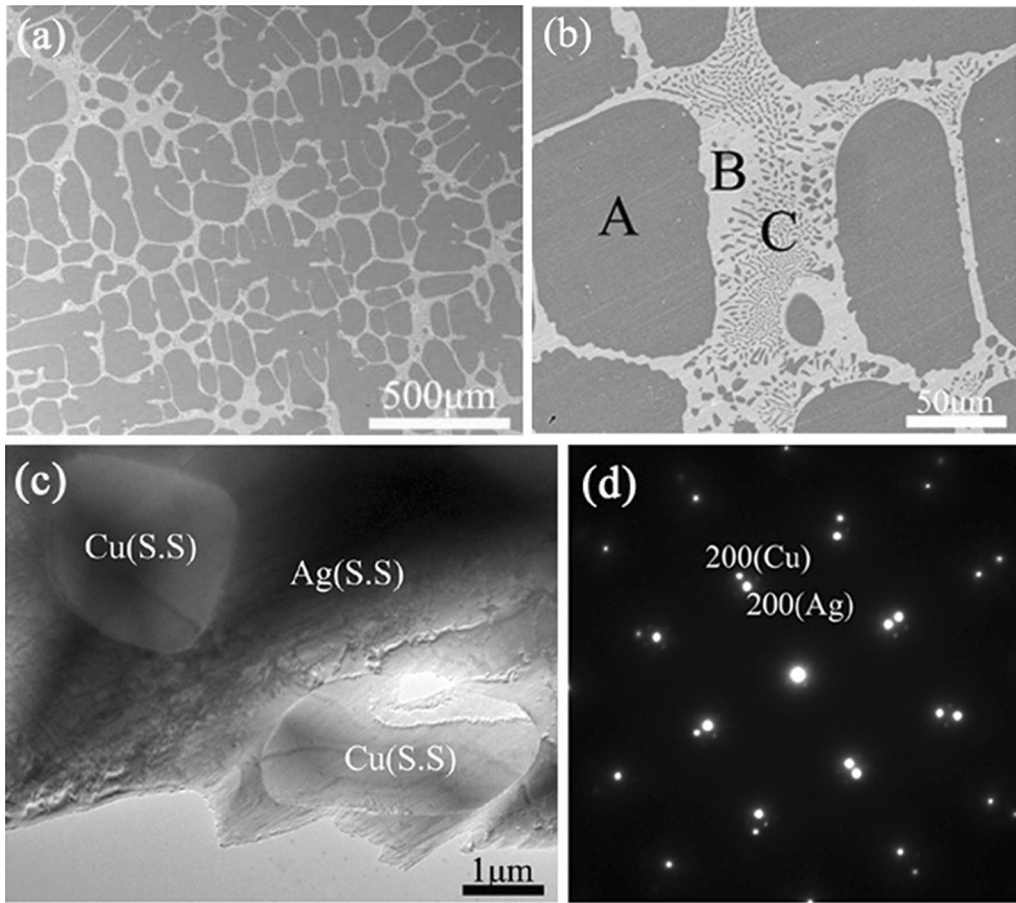


Fig. 5—(a) Low-magnification SEM image of layer I; (b) high-magnification view of layer I; (c) TEM image of eutectic structure, denoted as (B + C) in (b); and (d) SAED pattern of [001] zone axis showing that the Ag(S.S) and Cu(S.S) in eutectic structure have cubic-on-cubic crystallographic orientation.

**Table I. Average Chemical Compositions of Each Region in Layer I**

Interface Shape	Elements (At. Pct)			Ti	Possible Phase	Crystal Structure
	Region					
Conical	A	91.48	5.98	2.54	Cu(S.S)	$\alpha_p + \beta_{II}$
	B	6.68	93.32	0	Ag(S.S)	$(\alpha + \beta)_e + \alpha_{II}$
	C	96.55	2.72	0.73	Cu(S.S)	
Straight	A	94.00	4.41	1.59	Cu(S.S)	$\alpha_p + \beta_{II}$
	B	8.07	91.93	0	Ag(S.S)	$(\alpha + \beta)_e + \alpha_{II}$
	C	92.84	4.89	2.27	Cu(S.S)	

composition. Therefore, this typical microstructure can be well elucidated by a Ag-Cu binary phase diagram. When the molten liquid with hypereutectic composition began to solidify as the temperature decreased, the primary Cu solid solution ( $\alpha_p$ ) precipitated first; these Cu solid solutions are known as Cu-based dendrites. As the temperature reached about 1053 K (780 °C), the remnant liquid with the eutectic composition began to precipitate Ag-Cu eutectic structure (denoted as  $(\alpha + \beta)_e$ ). Figure 5(c) shows the TEM microstructure of the Ag-Cu eutectic structure, as noted in Figure 5(b). The composite selected area electron diffraction (SAED) pattern of the [001] zone axis in Figure 5(d) reveals the typical cubic-on-cubic crystal relationship of the Cu and

Ag solid solutions in the Ag-Cu eutectic structure (marked A and B). This cubic-on-cubic crystal relationship was also confirmed by SAED referring to zone A ( $\alpha_p$ ) and zone B ( $\beta$ ) (Figure 5(b)).

Further TEM observation found that there were also some Ag solid solution particles in zone A and some Cu solid solution particles in zone B, although the quantity of Cu solid solution in zone B was small. From the Ag-Cu binary phase diagram, it is clear that when the temperature further decreases from the eutectic temperature, there are some secondary Ag(S.S) ( $\beta_{II}$ ) and Cu(S.S) ( $\alpha_{II}$ ) precipitates from the primary Cu(S.S) ( $\alpha_p$ ) and Ag(S.S) ( $\beta$ ) matrix, respectively. Figures 6(a) and (b) show the micrographs of these secondary solid

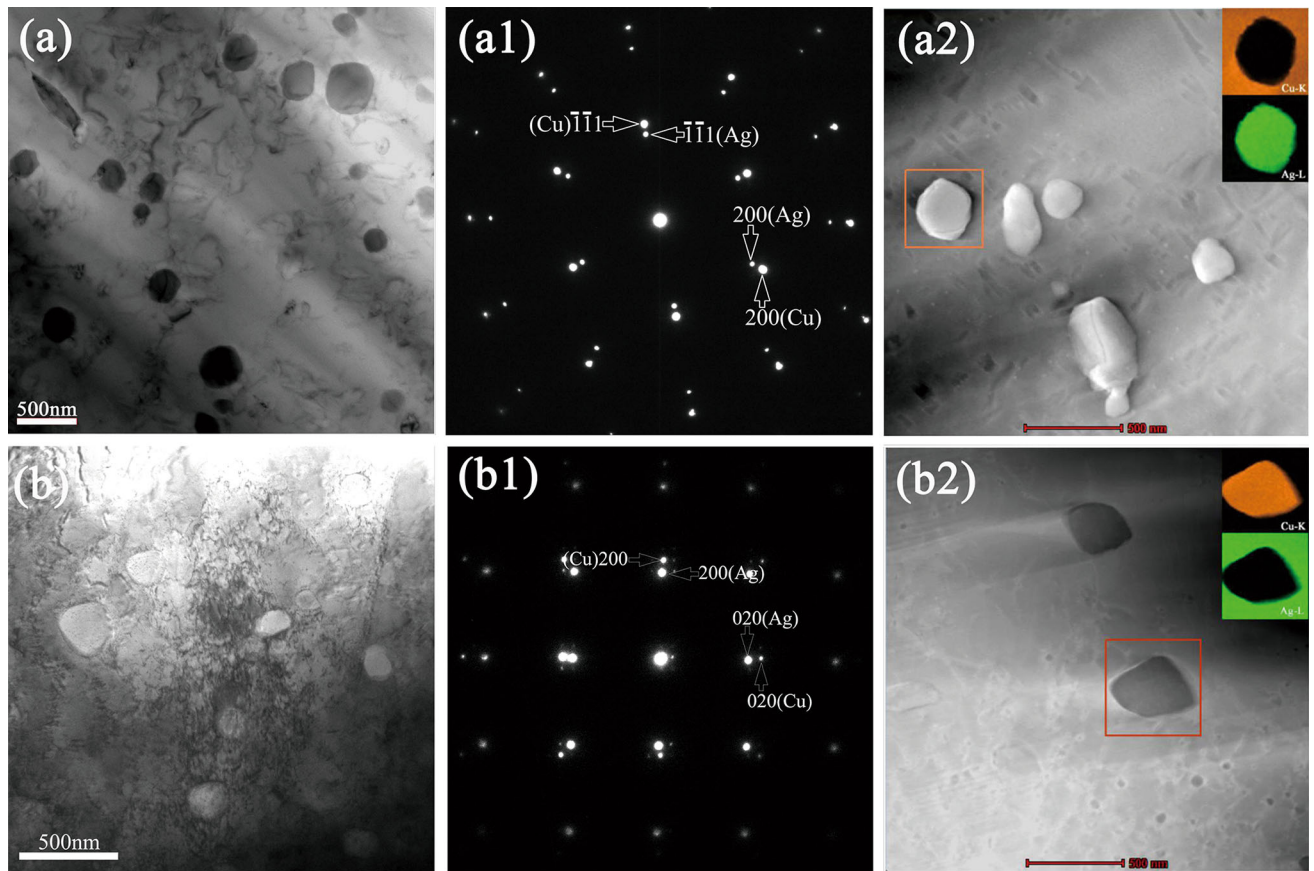


Fig. 6—Microstructure details of layer I: (a) Ag(S.S) ( $\beta_{II}$ ) precipitates from primary Cu(S.S) ( $\alpha_p$ ) in zone A, (a1) the corresponding SAED pattern of [110] zone axis; (b) Cu(S.S) ( $\alpha_{II}$ ) precipitates from Ag(S.S) ( $\beta$ ) matrix in zone B, (b1) corresponding SAED pattern of [001] zone axis. (a2) and (b2) Corresponding STEM images, respectively; insets are the element mappings of the precipitated particles.

solution particles, respectively. The composite SAED patterns in Figures 6(a1) and (b1) show that the crystallographic orientation relationship between the secondary solid solution and primary solid solution is highly coherent. The scanning transmission electron microscopy (STEM) micrographs of secondary Ag(S.S) ( $\beta_{II}$ ) and Cu(S.S) ( $\alpha_{II}$ ) particles are shown in Figures 6(a2) and (b2), respectively. The inserts are EDS element mappings. From the preceding analysis, it can be concluded that in layer I a cubic-on-cubic orientation relationship between Cu(S.S) and Ag(S.S) is confirmed:

$$[001]_{Ag} \parallel [001]_{Cu},$$

$$(hkl)_{Ag} \parallel (hkl)_{Cu} (h, k, l \text{ are all odd or all even}).$$

This typical microstructure in layer I should be conventional when AgCuTi is used as the active filler metal. In most cases, when AgCuTi was used as an active filler metal, the chemical ratio of silver and copper was 72:28 (wt), so the Ag-Cu eutectic structure was formed as the framework of a joint, and usually no hypereutectic solid solution was formed. The high Cu content of the braze alloy in our experiment is responsible for the microstructure difference in the brazing zone.

## 2. Microstructure of layer II

Figure 7(a) demonstrates the overview microstructure of layer II in the straight interface. It can be seen that this layer consists of mainly gray phase and a small amount of white phase, the white phase “islets” dispersed in gray phase. The high magnification presented in Figure 7(b) shows that there are no phases other than the white and gray phases. Figures 7(c) and (d) show the micrographs of layer II in the conical interface. It can be seen that there are many relatively large (micrometer scale) black precipitates distributed in the matrix. These precipitates have bacilliform, oblong, triangular, or irregular shapes, which appear to be preferentially formed within the white phase. The EDS analysis (Table II, the content of element O is not shown) shows that for both straight and conical interfaces in this layer, the gray phase consists mainly of Cu with a small quantity of Ti; the white phase consists mainly of Ag without any Ti. Therefore, the gray and white phases are probably Cu(S.S) and Ag(S.S), respectively. The microstructure details of the gray and white phases are similar to zones A and B in layer I.

Most of the precipitates consist of Cu and Ti, with a little oxygen, which indicates that these particles are presumably Cu-Ti or Cu-Ti-O compounds. If oxygen was introduced, two important ternary compounds,  $Cu_3Ti_3O$  and  $Cu_2Ti_4O$ , could be formed as common



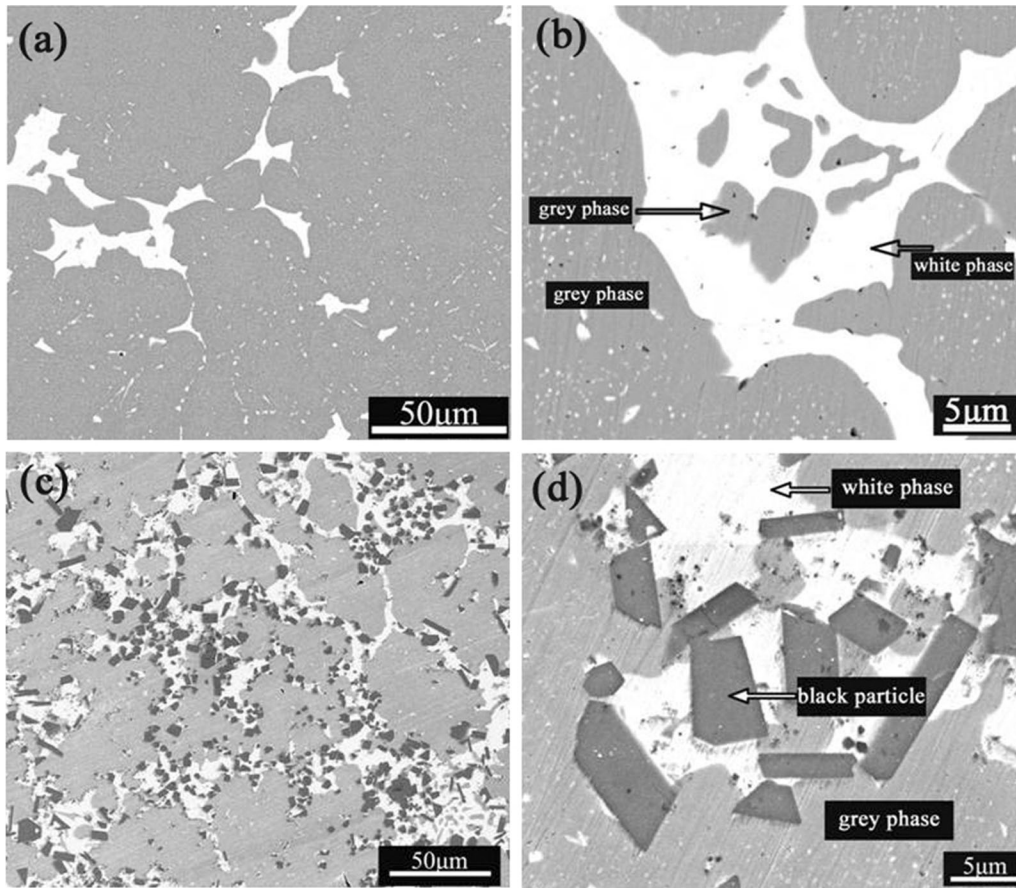


Fig. 7—SEM micrographs show the low- and high-magnification views of layer II: (a) and (b) straight interface joints; (c) and (d) conical interface joints.

Table II. EDS Analysis Results of Each Region in Layer II

Interface Shape	Elements (At. Pct) Region	Cu	Ag	Ti	Possible Phase
Conical	gray phase	96.17	2.10	1.73	Cu(S.S)
	white phase	7.79	92.21	0	Ag(S.S)
	black particles	51.13	0	48.87	Cu-Ti intermetallics
Straight	gray phase	93.38	5.58	1.04	Cu(S.S)
	white phase	8.56	91.44	0	Ag(S.S)

reaction products in the Cu-Ti-O system involving oxygen atmosphere and copper substrate when Ti-containing braze alloys were used. In the present study, the  $\text{Cu}_3\text{Ti}_3\text{O}$  ( $Fd\bar{3}m$ ,  $a = 1.1258$  nm) was identified and proved to be the predominant precipitates in layer II by means of SAED and EDS analyses. The  $\text{Cu}_3\text{Ti}_3\text{O}$  has a large range of size, from tens of nanometers to several micrometers. Figures 8(a) and (b) show the distribution of  $\text{Cu}_3\text{Ti}_3\text{O}$ . It can be seen that in Figure 8(a) large size  $\text{Cu}_3\text{Ti}_3\text{O}$  formed at the grain boundary between Ag(S.S) and Cu(S.S) and some small size  $\text{Cu}_3\text{Ti}_3\text{O}$  formed inside Ag(S.S). This finding can be seen more clearly in Figure 8(b) in which the  $\text{Cu}_3\text{Ti}_3\text{O}$  formed inside Ag(S.S). Figure 8(d) shows a series of SAED patterns with different zone axes rotated along  $[2-20]^*$  and  $[200]^*$  reciprocal axes. Figure 8(e) shows the EDS profile of

$\text{Cu}_3\text{Ti}_3\text{O}$ . The atom ratio of 1:1 for Cu and Ti was always deduced from the EDS results, and oxygen was invariably detected. Growth twins (Figure 8(c)) were always identified in large grain size of  $\text{Cu}_3\text{Ti}_3\text{O}$ , from which it is predictable that the  $\text{Cu}_3\text{Ti}_3\text{O}$  precipitates at brazing temperature and grows during cooling. Thermodynamic calculation makes it clear that Cu-Ti interactions are strong compared with Ag-Ti interactions.<sup>[17]</sup>

Furthermore,  $\gamma$ -TiO was also identified in layer II in the conical interface joint. The  $\gamma$ -TiO was also located inside the Ag (S.S) or at the grain boundaries between Ag (S.S) and Cu (S.S), as shown in Figure 9(a). Figure 9(b) shows the corresponding  $[001]$ ,  $[011]$ , and  $[111]$  SAED patterns of  $\gamma$ -TiO, respectively. The  $\gamma$ -TiO is fcc structure with the parameter  $a = 0.418$  nm, and the

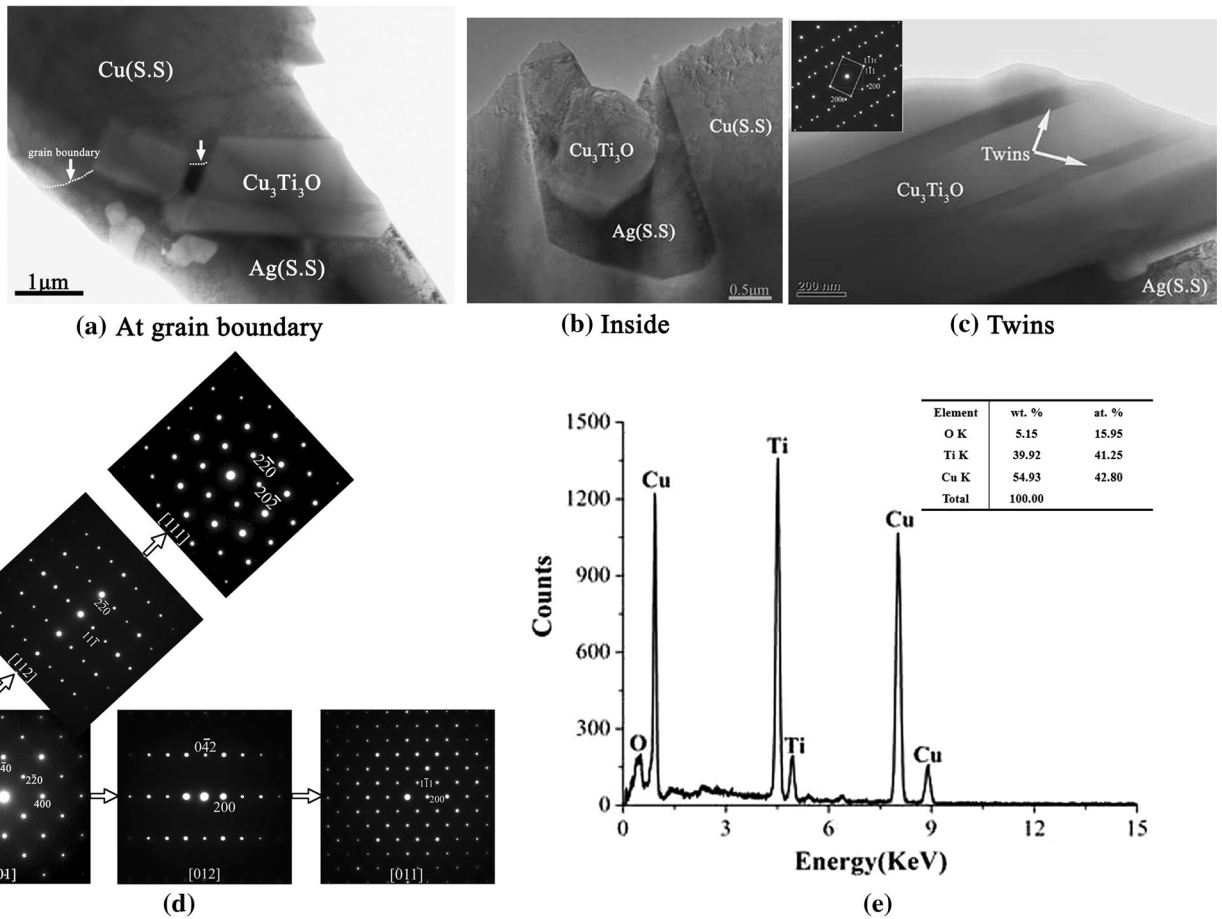


Fig. 8—TEM images show the location of  $\text{Cu}_3\text{Ti}_3\text{O}$  formed in layer II: (a) at the grain boundaries between  $\text{Ag}(\text{S.S})$  and  $\text{Cu}(\text{S.S})$ ; (b) inside  $\text{Ag}(\text{S.S})$ . (c) Twins of  $\text{Cu}_3\text{Ti}_3\text{O}$ ; (d) corresponding SAED patterns from [001], [012], [011], [112], and [111] zone axes of  $\text{Cu}_3\text{Ti}_3\text{O}$ ; and (e) EDS profile of  $\text{Cu}_3\text{Ti}_3\text{O}$ .

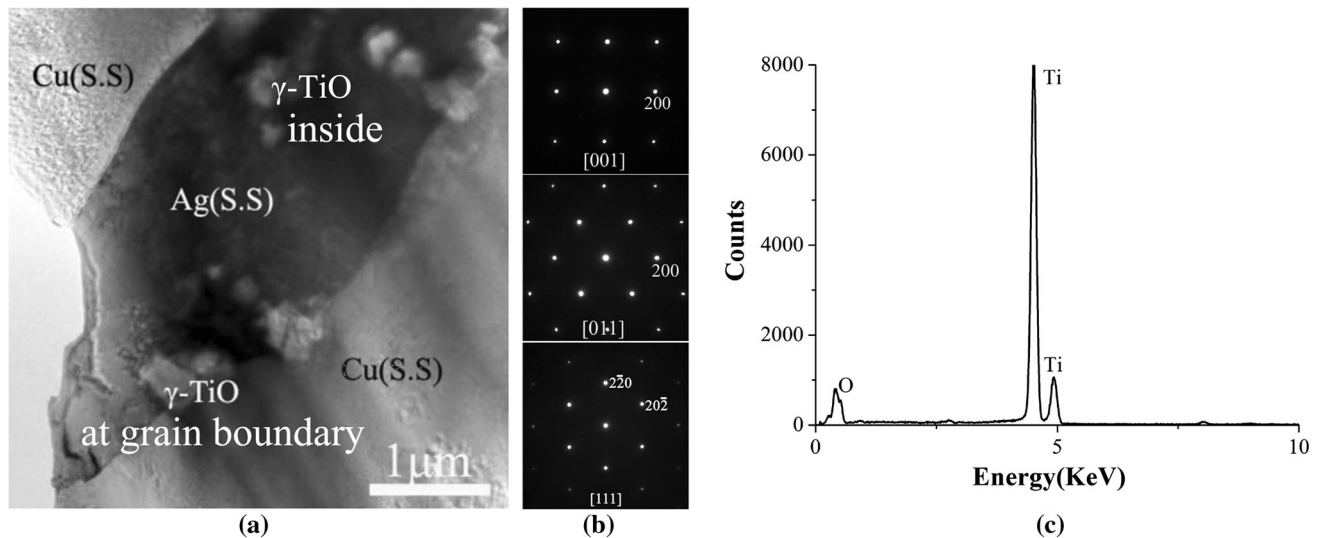


Fig. 9—(a) TEM image shows the  $\gamma\text{-TiO}$  formed inside the  $\text{Ag}(\text{S.S})$  or at the grain boundaries between  $\text{Ag}(\text{S.S})$  and  $\text{Cu}(\text{S.S})$ ; (b) corresponding SAED patterns from [001], [011], and [111] zone axes of  $\gamma\text{-TiO}$ , respectively; and (c) EDS profile of  $\gamma\text{-TiO}$ .

space group is  $Fm\text{-}3m$ . Figure 9(c) is the EDS profile of  $\gamma\text{-TiO}$ . It is known that titanium is a strong getter of oxygen and that titanium oxide can form at quite low

oxygen partial pressure. The surface of copper will be covered easily with copper oxides in spite of prior cleaning, and when the molten braze interacts with the



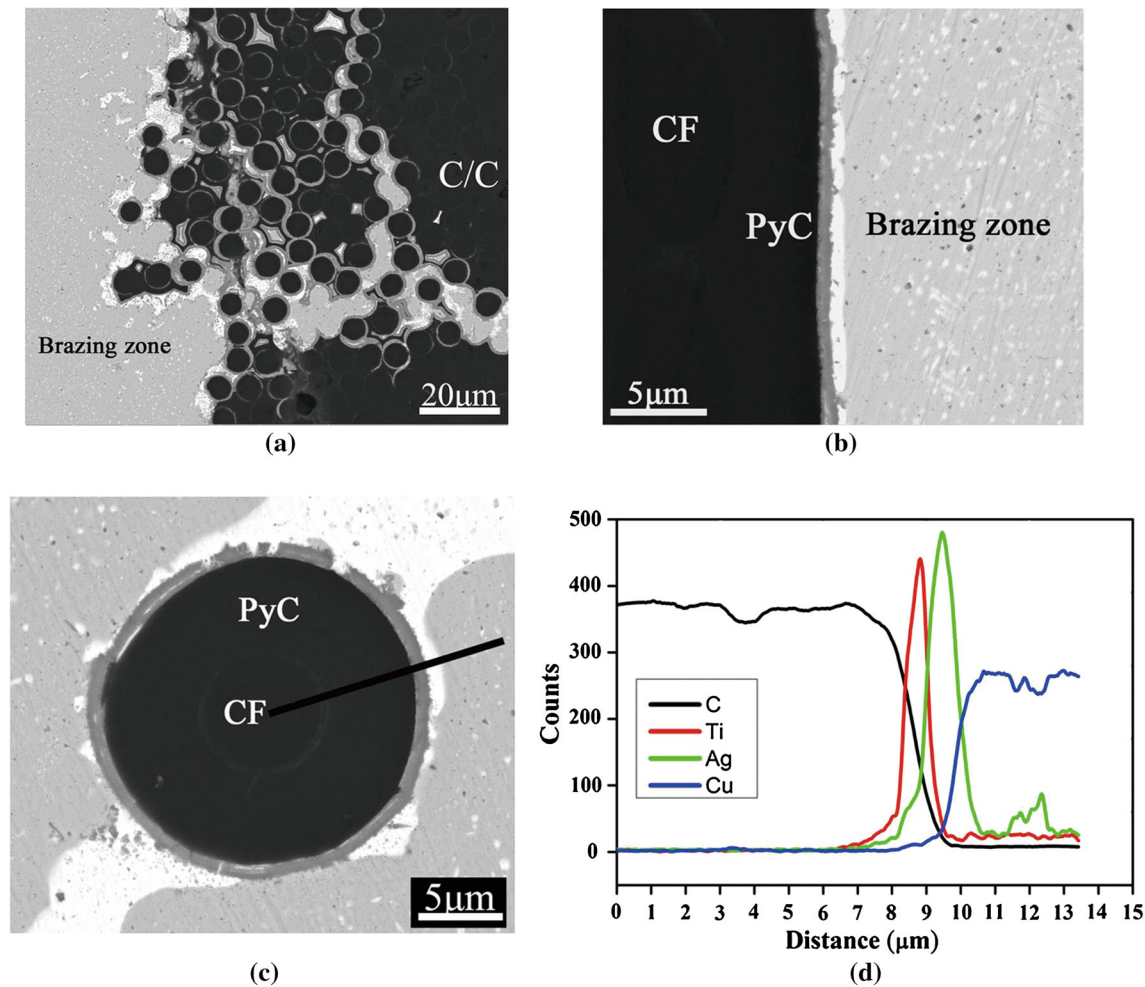


Fig. 10—(a) SEM micrograph of C/C composite/brazing zone; (b) backscattered electron image of PyC/brazing zone; (c) single CF and its PyC coating in brazing zone; and (d) EDS profile across the interface of brazing zone and PyC.

copper, the copper oxides will dissociate or dissolve into the molten braze first before interacting with pure copper. What is more, under the furnace atmosphere, a certain oxygen partial pressure is inevitable. Consequently, it was possible to form titanium oxide at the joint, especially at the interface of the braze zone and copper. Singh *et al.* predicted the existence of stable TiO at the C/C/metal joint.<sup>[1,8]</sup> At the Cu/AgCuTi interface, along with the dissolution of copper into molten braze and the introduction of oxygen, this interface region will be a Cu-rich Ag-Cu-Ti-O system. Kelkar and Carim<sup>[18]</sup> found that  $\text{Cu}_2\text{Ti}_4\text{O}$  and  $\text{Cu}_3\text{Ti}_3\text{O}$  were quite stable at 1198 K (925 °C) in an inert ambient. A large amount of oxide formed in this layer indicates that very low partial pressure of the oxygen environment will be requested for brazing as a result of the high activity of titanium.

### C. Interface Microstructure Between C/C Composite and Brazing Zone

Figures 10(a) and (b) show the interface microstructure of the C/C composite and brazing zone. Figure 10(a) shows the carbon fiber bundle/brazing zone interface, and Figure 10(b) shows the pyrolytic

carbon/brazing zone interface. No obvious microvoids and cracks were found in the contact region between the C/C composite and brazing zone. It was noticed in Figure 10(a) that the interfibers and pores between the carbon fiber and pyrolytic carbon (PyC) aggregated with white phase; this white phase proved to be Ag(S.S). It can be seen from Figure 10(b) that a reaction layer of gray phase formed at the surface of PyC obviously, followed by a layer of white phase. Figure 10(c) displays a single carbon fiber coated by PyC in the brazing zone. This phenomenon was caused by machining cones at the surface of C/C composites. The corresponding profile of EDS results on element distribution across the CF/PyC/brazing zone interface is shown in Figure 10(d). From this linear scan result, it can be seen that a reaction layer of less than 1- $\mu\text{m}$  thickness formed on the surface of PyC. From the EDS results, it is seen that the reaction layer is rich in Ti and C; the high Ti concentrations detected at the interface of the C/C composite and braze zone indicate the possible formation of a Ti-rich phase. Therefore, this reaction layer is TiC. The addition of titanium to braze improves wetting through the formation of titanium carbide at the interface. It is expected that the carbide formed at the surface of the C/C

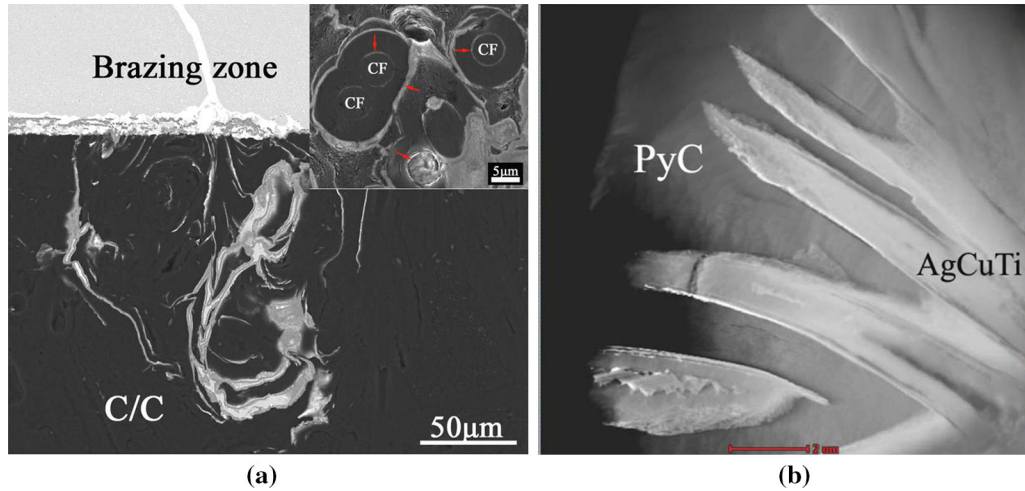


Fig. 11—(a) SEM image of the molten AgCuTi braze infiltrated into the micropores of the C/C composite. (b) STEM image shows the details of molten AgCuTi braze infiltrated into the micropores in PyC.

composite plays an important role in the brazing process. The element Ag was detected at the reaction layer. This means that the reaction products may disperse in Ag(S.S). What is more, as shown in Figures 10(a) through (c), the reaction layer is always followed by Ag(S.S) at the brazing zone. This phenomenon indicates that Ag may promote the formation of TiC layer.

Besides, the infiltration of pores in C/C composites by the molten AgCuTi has occurred. As is well known, there are intrinsic microcracks and pores in C/C composites, and when the filler metal melts, it infiltrates into the C/C composites through these microgaps. Figure 11(a) shows the morphology of molten metal impregnating in the microvoids and pores of the PyC and interfibers, forming the “pinning structure.” It was found that at some places an infiltration depth of 100  $\mu\text{m}$  or even more was observed. This infiltration phenomenon was more obvious in the conical interface due to interface machining. The insert in Figure 11(a) shows that not only the pores in PyC but also the circular gaps between PyC and carbon fibers (CFs) or the holes caused by the pulling out of CFs can be infiltrated by molten AgCuTi. Figure 11(b) shows the high-angle annular dark-field image of molten AgCuTi infiltrated into the pores in PyC. The high wettability of molten metal containing Ti allows the infiltration of these pores, and the capillary infiltration plays an important role in this progress.<sup>[10,16]</sup> This infiltration progress was mainly controlled by reaction rather than viscous flow.

#### D. Mechanical Properties of the Joints

The four-point bending test was performed in order to determine the strength and fracture toughness of the joint. Figure 12 shows the four-point bending strength of joints with straight and conical interface shapes. As can be seen from the bar graph, the average and maximum strengths of the joint with conical interface are 52 and 63 MPa, respectively. In contrast, the

average and maximum strengths of the joint with straight interface are 14 and 17 MPa, respectively. Hence, the average strength after interface structure design improves 3.7 times more than the common brazing joint strength. Both straight and conical interface joints invariably failed at the C/C composite part during bend testing.

## IV. DISCUSSION

### A. Effect of Ag on the Interfacial Reaction

Tables I and II show that no Ti was detected in the Ag solid solution in layers I and II. The quite small solubility of Ti in Ag is attributed to the mutual exclusion between the Ag and Ti elements. As shown in Section III-B, Ag has a great effect on the formation of compounds and on the interface microstructure of the brazing zone and C/C composite. It is worth noting that compounds formed at low Ti concentration; what is more, all of the compounds were precipitated just inside Ag (S.S) or at the grain boundaries between Cu(S.S) and Ag (S.S) (Figures 8 and 9). Figure 13(a) schematically shows the location of the compounds in layer II. As shown in Figure 10, a Ag layer was always found between the reaction layer and Cu(S.S). The high Ag content was also detected in the reaction layer. All of these findings suggest that the existence of Ag probably concerns the activity of Ti and subsequently promotes the reaction involving Ti.

In brazing ceramics to metals, the chemical activity of Ti in the liquid braze is usually the most important factor that determines the reaction products formed at the brazing alloy/metal interface.<sup>[19]</sup> The intermetallic compound formation in the AgCuTi braze could occur at a much lower Ti concentration, while in the binary Cu-Ti alloy, the compound  $\text{CuTi}_4$  appears only with a Ti concentration of at least 15 wt pct at  $T \approx 1153$  K (880 °C).<sup>[17]</sup> In the present study, the formation of Cu-Ti-O compounds or other intermetallics may be closely aligned with the Ag element. The examination of

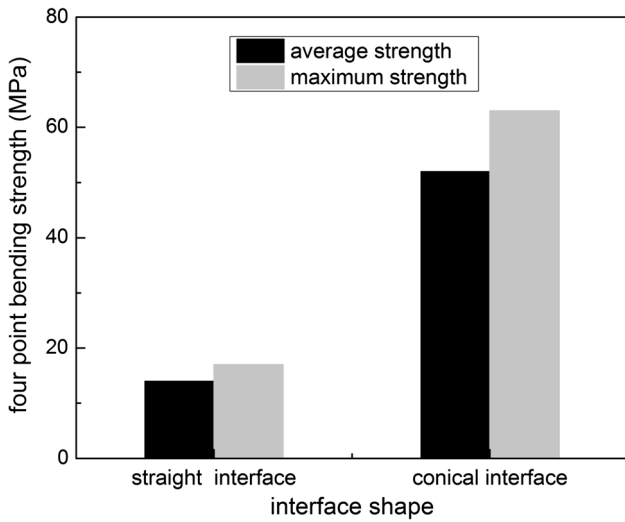


Fig. 12—Four-point bending strength of the joints with straight and conical interface.

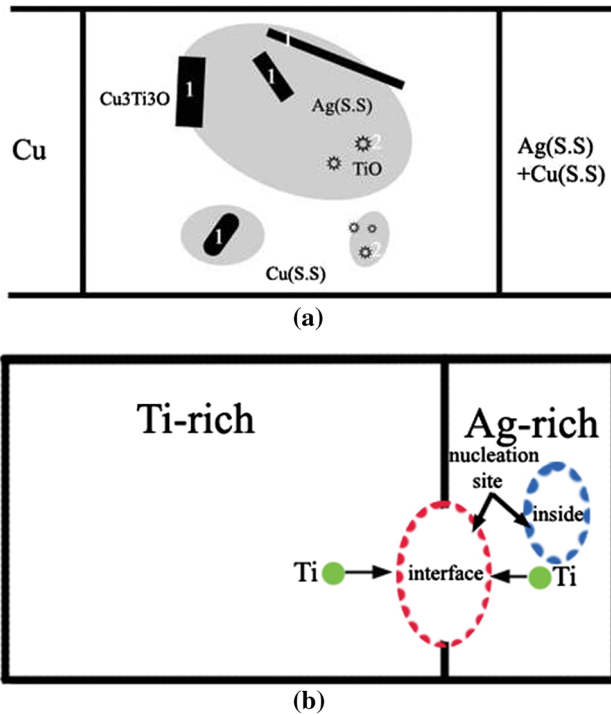


Fig. 13—(a) Schematic diagram of the location of the compounds formed in layer II during brazing. 1:  $\text{Cu}_3\text{Ti}_3\text{O}$ , 2:  $\gamma\text{-TiO}$ . (b) Schematic shows the nucleation position of the compounds at the interface between Ti-rich and Ag-rich liquid or inside the Ag-rich liquid.

mixing enthalpies in the AgCuTi system has proven that the presence of Ag in the liquid increases the thermodynamic activity of Ti<sup>[20–22]</sup> and, therefore, promotes the formation of intermetallic compound. The liquid Ag-Cu-Ti system is an important random substitutional solution phase. According to the regular solution approximation model, the Gibbs energy  $G_m^\Phi$  of such a phase can be described by

$$G_m^\Phi = \sum_i x_i^\Phi G_i^\Phi + RT \sum_i x_i^\Phi \ln(x_i^\Phi) + {}^{\text{ex}}G_i^\Phi \quad [1]$$

where  $x_i^\Phi$  is the molar fraction of component  $i$  in state  $\Phi$ ;  $\sum_i x_i^\Phi G_i^\Phi$  represents the contribution of pure components of the phase to the total Gibbs energy;  $RT \sum_i x_i^\Phi \ln(x_i^\Phi)$  is the ideal mixing contribution; and  ${}^{\text{ex}}G_i^\Phi$  is the excess Gibbs energy, which represents any interaction between components in the phase. The excess Gibbs energy  ${}^{\text{ex}}G_i^\Phi$  can be described by the expression

$${}^{\text{ex}}G_i^\Phi = \sum_i^{n-1} \sum_{j=i-1}^n x_i^\Phi x_j^\Phi L_{ij}^\Phi \quad [2]$$

where  $L_{ij}^\Phi$  is the interaction parameter between elements  $i$  and  $j$  that can be expanded as

$$L_{i,j}^\Phi = \sum_k L_{i,j}^{\Phi,k} (x_i^\Phi - x_j^\Phi)^k \quad [3]$$

$$L_{i,j}^{\Phi,k} = {}^k a + {}^k b T \quad [4]$$

Here, for simplicity, only Cu-Ti and Ag-Ti binary systems were considered to examine the effect of Cu and Ag on the activity of Ti. According to the data obtained from Arroyave<sup>[23]</sup> and from Dezellus,<sup>[24]</sup> the interaction parameters  $L_{\text{Ag,Ti}}^{\text{liq}}$  and  $L_{\text{Cu,Ti}}^{\text{liq}}$  could be calculated by Formulations [3] and [4]:

$$L_{\text{Ag,Ti}}^{\text{liq}} = 25,632 - 327(x_{\text{Ag}}^{\text{liq}} - x_{\text{Ti}}^{\text{liq}}) \quad [5]$$

$$L_{\text{Cu,Ti}}^{\text{liq}} = -19,330 + 7.651T + (9382 - 5.448T)(x_{\text{Cu}}^{\text{liq}} - x_{\text{Ti}}^{\text{liq}})^2 \quad [6]$$

In the regular solution model,

$$RT \ln \frac{a_{\text{Ti}}}{x_{\text{Ti}}} = (1 - x_{\text{Ti}})^2 L_{\text{Ag,Ti}}^{\text{liq}} \quad [7]$$

$$RT \ln \frac{a_{\text{Ti}}}{x_{\text{Ti}}} = (1 - x_{\text{Ti}})^2 L_{\text{Cu,Ti}}^{\text{liq}} \quad [8]$$

The relationship between activity and the activity coefficient is

$$\gamma_i = \frac{a_i}{x_i} \quad [9]$$

Combining Formulations [5] through [9], taking the temperature as 1183 K (910 °C), the theoretical variation of activity and the activity coefficient of Ti in Cu-Ti and Ag-Ti solutions as a function of the mole fraction of Ti could be calculated (Figure 14). It can be seen that the activity and the activity coefficient of Ti in



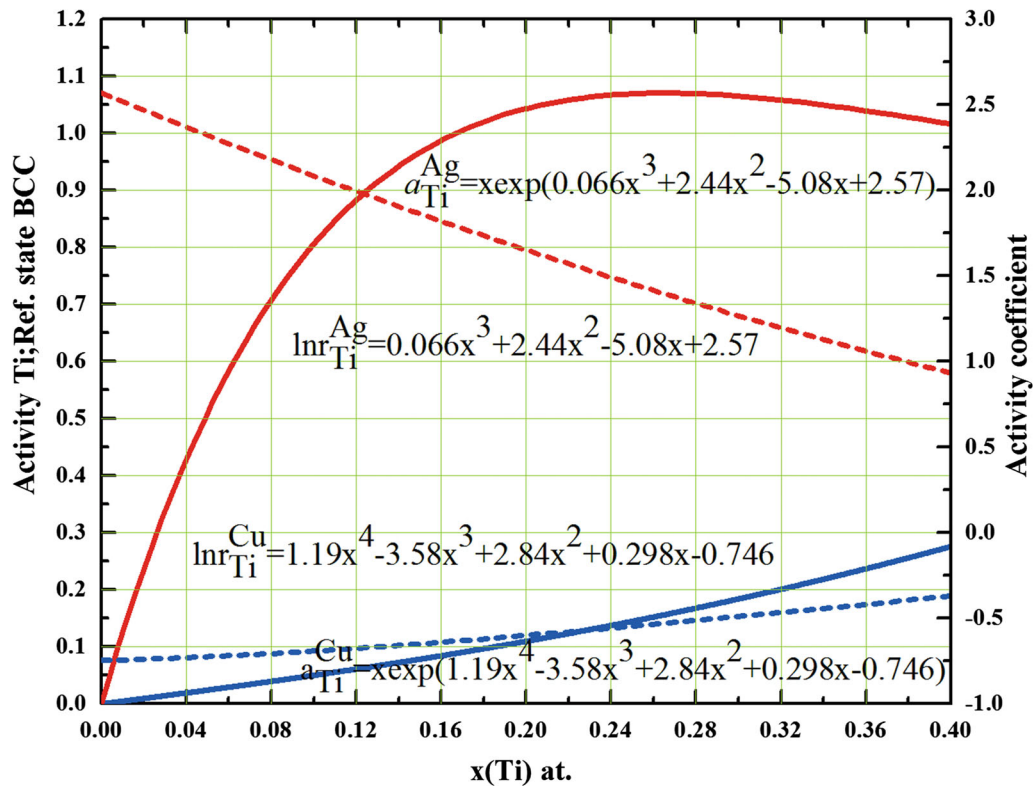


Fig. 14—Activity and activity coefficient of Ti as a function of  $x$  (Ti at.) at 1183 K (910 °C) in Cu-Ti and Ag-Ti liquid solution systems, respectively.

the Ag-Ti solution are rather large compared with those in the Cu-Ti solution. It should be noted that in our study the concentration of Ti in Cu melt or Ag melt is quite small.

As mentioned previously, from the position of compounds formed in layer II, it can be concluded that the nucleation sites of these compounds are either inside Ag-rich liquid or at the interface between Ti-rich and Ag-rich liquids, as shown in Figure 13(b). Thermodynamic calculations<sup>[24]</sup> show that the Ag-Cu-Ti system contains a liquid miscibility gap at a large composition range. The molten braze separates into two liquids, one is rich in Ag and the other is rich in both Cu and Ti. It is known that for a given component  $B$  in nonideal solution the chemical potential can be expressed by  $\mu_B = \mu_B^*(T, P) + RT \ln a_{B,x}$ . In liquid solution, the condition for Ti equilibrium in Ti- and Ag-rich liquids is  $\mu_{\text{Ti}}^{\text{Cu}} = \mu_{\text{Ti}}^{\text{Ag}}$ . Combined with the expression of chemical potential, it can be concluded that in equilibrium condition the Ti in Ti- and Ag-rich phases has the same activity  $a_{\text{Ti}}$ . Therefore, any composition fluctuation will increase the activity of Ti in Ag melt more intensely than that in Cu melt, which will promote the reaction between Cu and Ti. Also, the reaction needs the diffusion of Ti from Ti-rich liquid to Ag-rich liquid; hence, the nucleation sites are either inside Ag-rich liquid or at the interface between Ti- and Ag-rich liquids, as shown in Figure 13(b). These results also explain the large size  $\text{Cu}_3\text{Ti}_3\text{O}$  formed at the grain boundaries between Cu(S.S) and Ag(S.S). Based on the

thermodynamic description made available, the existence of Ag can significantly enhance the activity of Ti, and its value increases with an increase in Ag concentration, making it preferential for Ti to react with carbon. It can be deduced that the molten Ag with a small amount of Ti tends to segregate at the place where reaction occurs, which is why the Ag(S.S) can be seen beside the reaction layer (Figure 10).

## B. Formation Mechanism of the Joints

Based on closer microstructural analysis of the brazed joint, a possible mechanism of the formation process of the conical interface joint was proposed. The entire process can be divided into four stages (Figure 15). Physical contact occurs before melting of the braze alloy. As the temperature increases, both the brazing alloy and base material begin to expand. Consequently, small plastic deformation is created between the brazing alloy and base material, and this results in intimate contact between them. This temperature rise process also cleans the surface of the brazing alloy and base material before melting. When the temperature reaches a certain point, the AgCuTi foil begins to melt, and as the temperature increases, the alloy finally completely melts. During this melt process, atom diffusion occurs in the liquid. Titanium diffuses toward the C/C composite and reacts with carbon to form Ti carbide at the surface of the C/C composite. The liquid containing Ti spreads into the holes and gaps of the C/C composite to form

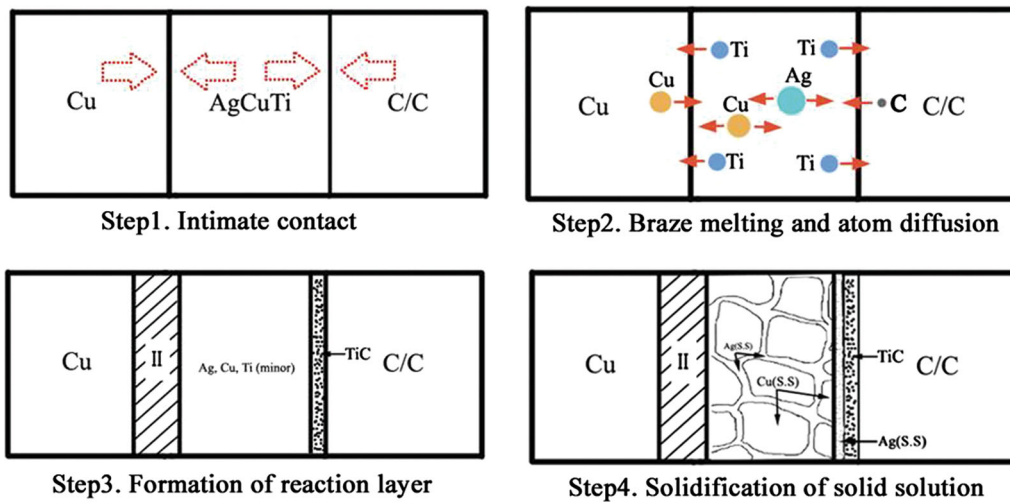


Fig. 15—Braze process divided into four steps factitiously to comprehend the mechanism of the braze process.

the so-called pinning structure under the action of capillarity. At the same time, Cu and Ag atoms move freely. The consumption of titanium results in depletion of the titanium content in the molten braze. Therefore, the concentration of titanium in the liquid decreases gradually. Meanwhile, the copper substrate dissolves in the liquid, and the liquidity of this region near copper increases as a result of the dissolution of copper. The nucleation of Cu-Ti compounds and other oxides occurs preferentially near the Cu substrate, and the segregation of silver promotes this process. With the formation of Ti-containing compounds, the concentration of titanium in the liquid decreases further. As the temperature decreases, the formation of compounds grows and the excess copper precipitates in the form of dendrites; the remaining liquid solidifies at 1053 K (780 °C), forming the typical Cu-Ag eutectic microstructure in the middle of the brazing zone. In the straight interface joint case, the formation progresses in basically the same manner. No compounds are found in layer II in the straight interface joint mainly because of the low titanium concentration near the Cu side. There would be less melt filler metal overflow from the interface in the conical joint than in the straight case due to the infiltration of the conical area. Accordingly, there will be much more Ti left to diffuse to the copper side. Hence, layer I is wider in the conical case, and the corresponding Ti concentration will be higher than in the straight case at the copper side. The redistribution of titanium is noted to occur during the process of brazing. A major portion of Ti diffuses to the surface and the pores of the C/C composite and *in situ* reacts with carbon to form a TiC layer. Another portion of Ti diffuses to the Cu side and reacts to form Ti-containing compounds due to the existence of oxygen; a relatively small amount of Ti dissolves in Cu(S.S). Therefore, the content of 4.5 wt pct Ti in the brazing alloy is sufficient for the interaction with the C/C composite to form a carbide layer.

### C. Factors that Affect Mechanical Performance and the Failure Mode

Because of the difference in the physicochemical properties of the two joint parts, C/C and copper, as well as the AgCuTi filler metal, the joint strength cannot be determined only by the interface microstructure. The mechanical state would change as the interface shape changed from straight to conical, which would influence the joint strength. Yet it is difficult to decouple the interface microstructure from the mechanical state. In the present study, the effect of the interface microstructure was discussed in terms of joint strength. On the basis of the four-point bending strength tests analysis, the failure mode of the joint was proposed.

#### 1. Effect of interface microstructure

There are three factors that definitely contribute to the mechanical performance of the joint in terms of the interface microstructure. Undoubtedly, the reaction between carbon and titanium, which forms a metal-like bonding at the interface of the C/C composite and the brazing zone plays an important role in determining the joint strength. Therefore, the concentration of Ti in the braze is crucial for chemical reaction. If the content of Ti is too low, the concentration will not guarantee the formation of a continuous reaction layer; on the other hand, a superfluous content of Ti would lead to an intense interface reaction and also result in the formation of a mass of intermetallic compounds, which would be detrimental to the mechanical performance of the joint. However, in the current study, the morphology and thickness of the TiC reaction layer in both straight and conical joints were quiet similar and no obvious difference was found. Therefore, it can be concluded that the reaction between carbon and titanium probably is not responsible for the strength difference. Additionally, there are plenty of compounds formed in layer II near Cu for the conical interface joint. Most of these

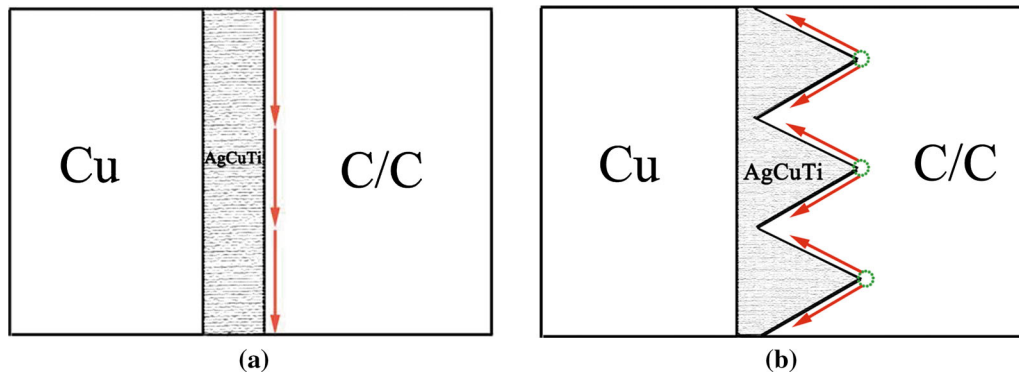


Fig. 16—(a) and (b) Schematics showing the failure mode of straight and conical interface joints, respectively. The bending mechanical properties test shows that fracture sites and crack propagation paths are different for straight and conical interface joints. The arrows indicate the crack location and propagation direction.

compounds are intrinsically brittle, and from a mechanical point of view, the formation of these compounds is expected to influence the metallurgical continuity across the joint and damage the interfacial ductility between the braze alloy and Cu. However, in the present study, this compound layer had no effect on the bonding strength of the joint since it was easier to fracture at the C/C composite side. That said this compound layer may reduce the assembly of thermal conductivity significantly, which is important when the assembly is used as a heat sink.

The other important factor is the formation of a special structure as a result of permeation of the braze melt into the pores and holes (or voids) of the C/C composite and its “pinning effect” between C/C composites and the impregnation metal. This special pinning structure will release the residual thermal stress induced by the mismatch of the dissimilar substrates and elevate the joining strength between the metal and C/C composites.<sup>[10]</sup> The impregnation of the pores and the formation of carbides results in a mechanical type joining, in which the joint strength does not rely only on interface adhesion but also on the interlocking of the C/C composite and braze.<sup>[25]</sup> Mechanical tests show that most fracture occurs in C/C composites, and in some cases, the failure occurs at the interface of the C/C composite and brazing zone; seldom is fracture propagated through the joint region.<sup>[3]</sup> This finding means that the interlocking region between C/C composites and the metal will play a key role in the joint strength. The surface of the C/C composite is coarse after micromachining, so it is easy to infiltrate by liquid filler through the role of capillary permeability, which would create some amount of pinning structure. It could be calculated from the scale of interface design in Figure 2 that the contact area between the C/C composite and molten braze in the conical interface is 1.3 times larger than that in the straight interface. Finally, the bonded area in the conical interface joint is much larger than that in the straight interface joint, which could reduce the residual stress. The ductile nature of layer I could adapt to part of the incompatibility between the two partners in thermal expansion and elastic deformation.

## 2. Failure mode of the joints

The four-point bending test has proven that both straight and conical interface joints fracture at the C/C composite side near the metal/carbon interface. The failure modes of the joints are different due to the difference in their interface shapes. The cracks preferably initiate at the C/C composite side near the metal/carbon interface. Figure 16(a) shows the failure mode for the straight interface joint. The arrows indicate the crack propagation direction. In this case, the bending strength is small. Figure 16(b) shows the failure mode of the conical interface joint. The cracks probably initiate at the tip of the cone and extend along the surface of the cone. The arrows indicate the direction of the fracture paths.

## V. CONCLUSIONS

1. Two surface configurations of C/C composite, straight and conical, were designed and machined before brazing to copper using an Ag-68.8Cu-4.5Ti (wt pct) alloy. Sound joints were obtained for both straight and conical interfaces following the normal brazing method.
2. The microstructures of both joints can be described as C/C composite/TiC/Ag(S.S)/layer I/layer II/Cu. In the conical interface case, reaction products of  $\text{Cu}_3\text{Ti}_3\text{O}$  and  $\gamma\text{-TiO}$  were formed inside Ag(S.S) or at grain boundaries between Ag(S.S) and Cu(S.S) in layer II. The thickness of the titanium carbide layer formed at the surface of C/C composite was approximately  $1\ \mu\text{m}$ . The infiltration of melt AgCuTi into the micropores of C/C composites occurred under the action of reaction and capillarity. The activity of Ti increases significantly by silver in the alloy and, as a result, facilitates the formation of both TiC- and Ti-containing compounds.
3. The average four-point bending strengths of the straight and conical interface joints are 14 and 52 MPa, respectively. The average joint strength of the conical interface improves 3.7 times over the common straight interface brazing joint. Different



fracture modes are proposed for both joints: (a) Straight interface—the cracks arise at the C/C side near the interface of the brazing zone and C/C composites; (b) Conical interface—the cracks arise at the tip of the cones and propagate along the conical interface near C/C composites.

### ACKNOWLEDGMENT

The financial support of the National Program on Key Basic Research Project (973 Program) (Grant No. 2011CB605803) is gratefully acknowledged.

### REFERENCES

1. M. Singh, T.P. Shpargel, G.N. Morscher, and R. Asthana: *Mater. Sci. Eng. A*, 2005, vol. 412, pp. 123–28.
2. Y. Qin and J. Feng: *Mater. Sci. Eng. A*, 2007, vols. 454–455, pp. 322–27.
3. P. Appendino, V. Casalegno, M. Ferraris, M. Grattarola, M. Merola, and M. Salvo: *Fus. Eng. Design*, 2003, vols. 66–68, pp. 225–29.
4. M. Salvo, V. Casalegno, S. Rizzo, F. Smeacetto, M. Ferraris, and M. Merola: *J. Nucl. Mater.*, 2008, vol. 374, pp. 69–74.
5. M. Singh, N.M. Gregory, and P.S. Tarah: *Mater. Sci. Eng. A*, 2008, vol. 498, pp. 31–36.
6. N.V. Moutis, C. Jimenez, X. Azpiroz, T. Speliotis, C. Wilhelmi, S. Messoloras, and K. Mergia: *J. Mater. Sci.*, 2010, vol. 45, pp. 74–81.
7. V. Casalegno, M. Salvo, and M. Ferraris: *Carbon*, 2012, vol. 50, pp. 2296–3306.
8. M. Singh, R. Asthana, and T.P. Shpargel: *Mater. Sci. Eng. A*, 2007, vols. 452–453, pp. 699–704.
9. Y. Qin and J. Feng: *Mater. Sci. Eng. A*, 2009, vol. 525, pp. 181–85.
10. H. Wang, J. Cao, and J. Feng: *Scripta Mater.*, 2010, vol. 63, pp. 859–62.
11. Y. Shen, Z. Li, C. Hao, and J. Zhang: *J. Eur. Ceram. Soc.*, 2012, vol. 32, pp. 1769–74.
12. G. Lin, J. Huang, H. Zhang, and X. Zhao: *Mater. Trans.*, 2006, vol. 47, pp. 1261–63.
13. M. Singh and R. Asthana: *Compos. Sci. Technol.*, 2008, vol. 68, pp. 3010–19.
14. N. Eustathopoulos, M. Nicholas, and B. Drevet: *Wettability at High Temperatures*, 2nd ed., Pergamon, Oxford, United Kingdom, 1999, pp. 363–65.
15. L. Yang, P. Shen, Q. Lin, F. Qiu, and Q. Jiang: *Mater. Chem. Phys.*, 2010, vol. 124, pp. 499–503.
16. W. Guo, Y. Zhu, L. Wang, Q. Ping, H. Kang, and P.K. Chu: *Mater. Sci. Eng. A*, 2013, vol. 564, pp. 192–98.
17. O. Kozlova, M. Braccini, R. Voytovych, N. Eustathopoulos, P. Martinetti, and M.-F. Devismes: *Acta Mater.*, 2010, vol. 58, pp. 1252–60.
18. G.P. Kelkar and A.H. Carim: *J. Am. Ceram. Soc.*, 1993, vol. 76, pp. 1815–20.
19. R. Arroyave and T.W. Eagar: *Acta Mater.*, 2003, vol. 51, pp. 4871–80.
20. KC Hari Kumar, I Ansara, P Wollants, and L Delaey: *Z. Metallkd.*, 1996, vol. 87, pp. 666–72.
21. M. Li, C. Li, F. Wang, and W. Zhang: *Comput. Coupling Phase Diagr. Thermochem.*, 2005, vol. 29, p. 269.
22. R. Hultgren: *Selected Values of Thermodynamic Properties of Binary Alloys*, ASM International, Metals Park, 1973.
23. R. Arroyave: Ph.D. Thesis, MIT, Cambridge, 2004, pp. 209–10.
24. O. Dezellus, R. Arroyave, and S.G. Fries: *Int. J. Mater. Res.*, 2011, vol. 102 (3), pp. 286–97.
25. C. Jimenez, K. Mergia, N.V. Moutis, X.A. Azpiroz, C. Wilhelmi, T. Speliotis, and S. Messoloras: *J. Mater. Eng. Performance*, 2012, vol. 21, pp. 683–89.